Enhancing CO−Water Mass Transfer by Functionalized MCM41 Nanoparticles

Haiyang Zhu,[†,‡] Brent H. Shanks,[‡] and Theodore J. Heindel*[,†]

Department of Mechanical Engineering, 2025 Black Engineering Building, and Department of Chemical and Biological Engineering, 2114 Sweeney Hall, Iowa State University, Ames, Iowa 50011

Organic groups are grafted to ∼250-nm-diameter MCM41 nanoparticles with a spherical morphology to enhance the CO−water volumetric mass-transfer coefficient (k_La) for synthesis gas fermentation. The results indicate that (i) ∼250-nm MCM41 nanoparticles show a higher k_La value than large silica particles (1.4 and 7 μm), (ii) surface hydroxyl groups on MCM41 nanoparticles play an important role in mass-transfer enhancement, (iii) organic groups grafted to MCM41 modify the mass-transfer enhancement, and (iv) mercaptan groups grafted to MCM41 show the most mass-transfer enhancement of ∼1.9 times that of no nanoparticle addition. The CO−water mass-transfer enhancement depends on the interaction between the nanoparticles and the CO molecules, which is influenced by the hydrophobicity of the nanoparticles and the functional group on the nanoparticles.

1. Introduction

Synthesis gas (syngas) derived from the gasification of coal, natural gas, or biomass is composed primarily of carbon monoxide (CO) and hydrogen (H_2), which can be fermented using microorganisms (e.g., *Rhodospirillum rubrum*) to produce a variety of fuels and chemicals such as ethanol, methane, and acetic acid.[1−4] Therefore, syngas fermentation is a potential pathway for converting biomass to a variety of fuels and chemicals because of its low cost and potentially high efficiency. The actual conversion efficiency depends on the microorganism and the desired product but can easily be 35% or higher.[5−8]

In syngas fermentation, carbon monoxide is the sole carbon source from which the microorganisms produce the desired chemicals. However, the solubility of CO in the aqueous medium is low, which minimizes the CO−liquid mass-transfer rate and limits the overall product yield.[2,9−11] For syngas fermentation to be successful, CO−liquid mass-transfer rates must be enhanced. However, limited attention has been paid to unique approaches for enhancing CO−liquid volumetric mass-transfer coefficients, which is the focus of this work.

In general, gas−liquid mass transfer is influenced by reactor type, power input, and system additives. Ungerman and Heindel[12] compared CO−water volumetric mass-transfer coefficients in a stirred-tank reactor using different impeller designs and schemes and found that the dual Rushton-type impeller scheme produced the highest volumetric mass-transfer coefficient. Compared to the standard (single) Rushton-type impeller scheme, the dual Rushton-type impeller scheme enhanced mass transfer by up to 27%. However, the dual Rushton-type scheme also required the most power input, which resulted in the lowest mass-transfer rate per unit power input. Others[13−18] have added surfactants, alcohols, salts, and small particles to increase gas−liquid mass-transfer rates. Olle et al.[19] synthesized magnetite (Fe_3O_4) nanoparticles coated with oleic acid and a surfactant and achieved a 600% enhancement in the oxygen−liquid mass-transfer rate in an agitated sparged reactor at nanoparticle volume fractions below 1%. Using an oxygen−liquid system, Littlejohns and Daugulis[17] determined that nylon-6,6 and glass beads enhanced the volumetric mass-transfer coefficient by up to 268%, whereas silicone rubber and styrene−butadiene copolymer particles reduced the volumetric mass-transfer coefficient. Others have also shown that gas−liquid mass-transfer coefficients can be enhanced through addition of small particles or catalysts.[14,18]

Beenackers and van Swaaij[20] reviewed the four possible mechanisms of gas−liquid mass-transfer enhancement when small particles are added to a system. Among them, the shuttle or grazing effect, in which small particles transport an additional amount of gas to the liquid bulk through adsorption in the gas−liquid diffusion layer and desorption in the liquid, is well-acknowledged. This method of enhancement is influenced greatly by particle size and surface characteristics (e.g., hydrophobic or hydrophilic). Although previous researchers using micro- and nanoparticles focused on enhancing oxygen−liquid mass transfer,[13−18] this method can be extended to CO−liquid mass-transfer enhancement.

Mesoporous silica materials (MCM41) have extensive adsorption capability because of their large BET surface areas (∼1000 m^2/g), and they can also be readily functionalized with organic groups to adjust the surface characteristics such as its hydrophobicity or hydrophilicity and acidity or basicity.[21−23] Hence, these materials are good candidates for enhancing the CO−liquid mass-transfer rate. In this work, MCM41 nanoparticles were synthesized with a spherical morphology and a diameter of ∼250 nm. Various organic groups such as methyl, carboxylpropyl, nitrilpropyl, and mercaptopropyl were then grafted to the MCM41 nanoparticles to adjust their surface properties with the intent of enhancing the CO−water volumetric mass-transfer coefficient (k_La).

2. Experimental Procedures

2.1. Synthesis of MCM41 Nanoparticles. MCM41 nanoparticles were synthesized following the procedures of Deng et al.;[24] only a summary is provided here. The nanoparticles were synthesized by first dissolving 1.2 g of cetyltrimethylammonium bromide (CTAB, Aldrich) into a mixture of 105 mL of deionized water and 45 mL of ethanol (100%). The solution was then stirred vigorously at 500 rpm while 2 mL of ammonium hydroxide (Sigma-Aldrich) was added. The solution was heated to 30 °C, 5.46 mL of tetraethyl orthosilicate (TEOS, 98%) was then added, and the mixture was stirred at 500 rpm for 3 h at 30 °C. The resulting slurry was filtered with a 4−5.5-μm

* To whom correspondence should be addressed. Fax: +1 515 294 3261. E-mail: theindel@iastate.edu.
[†] Department of Mechanical Engineering.
[‡] Department of Chemical and Biological Engineering.

10.1021/ie800238w CCC: $40.75
Published on Web 09/20/2008

Buchner funnel with a fritted disk, washed with ethanol, and then allowed to dry overnight at room temperature. The dried particulate cake that formed was ground with a mortar and pestle, sonicated for 1 h in approximately 200 mL of ethanol, refiltered, and dried overnight. The as-synthesized sample was then refluxed in 150 mL of acid/ethanol solution per gram of sample at 60 °C for 6 h to remove any remaining surfactant (CTAB). The acid/ethanol solution was derived from HCl diluted in ethanol (1:100 v/v). This extraction procedure was repeated twice. Finally, the sample was again filtered with a 4−5.5-μm Buchner funnel with a fritted disk, washed with ethanol, and dried overnight at 90 °C.

2.2. Synthesis of Functionalized MCM41 Nanoparticles. In the present work, methyl (Me), aminepropyl (AP), carboxylpropyl (CP), nitrilpropyl (NP), mercaptopropyl (MP), and mercaptoundecyl (MU) groups were grafted onto the MCM41 nanoparticle surface. During the MCM41 synthesis procedure described in the preceding section, the requisite amount of silane with the desired organic group was added into the mixture after the prehydrolysis of TEOS after about 30 min of stirring. The samples are denoted in this study as XXMCM41(x:y), where XX represents the desired organic group and x:y represents the molar ratio of the respective organic group to TEOS. For example, MeMCM41(1:9) represents methyl groups grafted to MCM41 nanoparticles at a molar ratio of 1 part MeTEOS to 9 parts TEOS.

2.3. Nanoparticle Characterization. Brunauer−Emmett−Teller (BET) surface areas were measured on a Micromeritics ASAP 2020 system, and the resulting pore volumes and pore size distributions were calculated by the BET and Barrett−Joyner−Halenda (BJH) methods, respectively. The measurements were taken at −196 °C. All samples were degassed at 100 °C for 5 h before measurement. The hydrophobic property was characterized on a Perkin-Elmer TGA7 instrument by the mass loss of water physically adsorbed on the samples. Scanning electron microscopy (SEM) images were recorded on a JEOL 840A instrument using the gold-coating sample preparation procedure. Nanoparticle size distributions (PSDs) were measured on a Malvern ZETA SIZER Nano-ZS90 instrument.

In situ Fourier transform infrared (FTIR) spectroscopy of CO adsorption was carried out on a Nicolet 5700 FTIR instrument (Thermo Electron Corporation) at 4 cm^{-1} resolution. A thin, but intact, self-supporting sample wafer (∼15 mg) was prepared following the procedure of Zhu et al.[25] and mounted inside a high-temperature cell. The wafer was pretreated at 100 °C for 1 h by flowing N_2 over the wafer surface to remove any physically adsorbed water and then cooled to room temperature. Subsequently, CO was introduced into the high-temperature cell and kept at atmosphere pressure for 30 min. The sample wafer was then heated to 100 °C and finally cooled to room temperature under a N_2 stream. The resulting spectra were recorded at several temperatures of interest.

2.4. Determination of CO−Water Volumetric Mass-Transfer Coefficients (k_La). CO−water volumetric mass-transfer coefficients were measured in a 250-mL microreactor filled with 200 mL of nanopure water (Figure 1). For all experiments in this study, a stir bar was agitated with a magnetic stirrer at a constant speed of 300 rpm, and the CO flow rate was held constant at 180 mL/min. The CO−water k_La values were determined by introducing a step change in CO concentration and then measuring the dissolved CO concentration as a function of time. N_2 was initially sparged through the microreactor gas inlet for 20 min before the gas was switched to CO. A single 10-μL liquid sample was withdrawn every 30 s from the sample port using gastight syringes from Hamilton; 13 liquid samples were collected for each test. After 20 min of CO sparging, three additional CO samples were collected to determine the steady-state (saturated) dissolved CO concentration. Dissolved CO concentrations were determined using a myoglobin−protein (Sigma-Aldrich) assay following the technique refined by Jones.[26] A Cary-50 Bio spectrophotometer from Varian (Mulgrave, Victoria, Australia) was used to assess the dissolved CO concentration in the liquid samples.

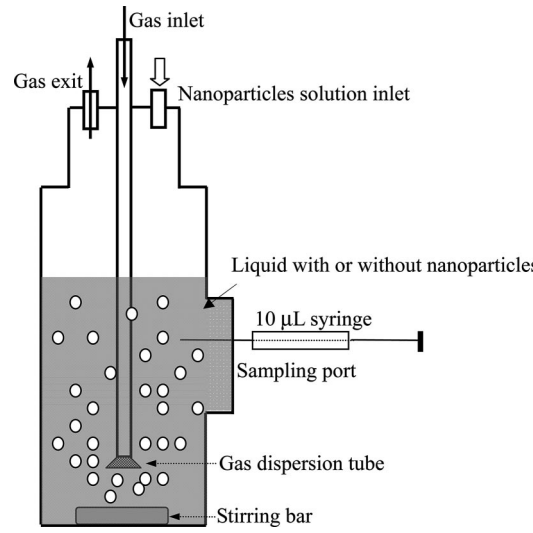

Figure 1. Schematic of the CO−water mass-transfer experimental apparatus.

The effect of nanoparticle addition on the CO−water volumetric mass-transfer coefficient was determined in the same vessel. The desired nanoparticle concentration was dispersed via sonication into 3 mL of deionized water. CO−water volumetric mass-transfer coefficients without nanoparticles (k_La_0) were recorded as a reference for each sample. A syringe was then used to remove 3 mL of liquid, and 3 mL of the desired nanoparticle concentration was added to the microreactor through the nanoparticle solution inlet port. The CO−water volumetric mass-transfer coefficient with nanoparticles (k_La_p) was then determined following the procedure described above. The enhancement in CO−water mass transfer (E) was defined as

$$E = \frac{k_La_p}{k_La_0} \tag{1}$$

2.5. Error Quantification. For the given experimental conditions, the percent standard error values in k_La for the CO−water-only system was estimated to be 7.6%, based on nine samples. The major sources of error in the reported k_La values derive from the measurement of dissolved CO concentrations. These measurements are influenced by the potential for gas entrainment in the sampling syringe, the limited number of samples in the k_La determination, and the lack of automation in the measurement procedures. Gas entrainment in the syringe would produce concentration values much higher than expected (i.e., the concentration did not gradually increase with time and one concentration value was much higher than all the rest); these readings were discarded. The k_La values were determined from at least 13 concentration measurements as a function of time, which were adequate assuming a first-order response. Finally, by refining the sample acquisition techniques, the impact of nonautomated sampling was minimized. It was assumed that

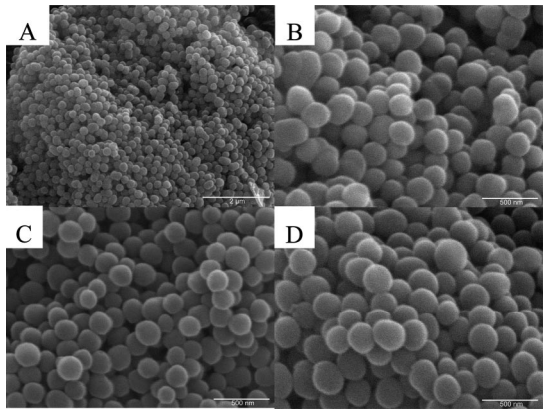

Figure 2. SEM images of MCM41 materials without or with methyl groups: (A) MCM41, scale bar = 2 μm; (B) MCM41, scale bar = 500 nm; (C) MeMCM41 (1:9), scale bar = 500 nm; and (D) MeMCM41 (3:7), scale bar = 500 nm.

Table 1. BET Surface Area and TGA Water Desorption Data for MeMCM41 Samples

sample	BET surface area (m^2/g)	H_2O desorption (wt %)
MCM41	1200	4.0
MeMCM41(1:49)	1100	14.3
MeMCM41(1:19)	1300	4.4
MeMCM41(1:9)	1400	3.1
MeMCM41(2:8)	1300	2.6
MeMCM41(3:7)	1200	2.8

the errors in the k_La measurements were similar when nanoparticles were added to the system.

3. Results and Discussion

Figure 2 shows SEM images of MCM41 nanoparticles without and with methyl groups grafted to the particles. The particles in Figure 2A,B have a spherical morphology with a diameter of ~250 nm, which was supported by particle size distribution measurements. After different methyl group loadings were grafted onto the MCM41 particles, yielding MeMCM41(1:9) (Figure 2C) and MeMCM41(3:7) (Figure 2D), the resulting particles had a morphology and size similar to those of the MCM41 particles. As shown in Table 1, the BET surface areas of MCM41 and the various MeMCM41 samples were ~1300 m^2/g. These results suggest that the grafting of various loadings of methyl groups onto MCM41 nanoparticles has a negligible effect on particle morphology, size, and surface area compared to pure MCM41 nanoparticles for the current synthesis conditions.

Figure 3 shows that the CO−water volumetric mass-transfer enhancement was influenced by the silica particle size and nanoparticle preparation procedures. When the surfactant involved in the MCM41 synthesis was removed by extraction, enhancement increased from 1 to 1.55 as the nanoparticle concentration increased from 0 to 0.4 wt %. For large silica particles with diameters of 1.4 and 7 μm, the maximum enhancements were 1.29 and 1.01, respectively, when the particle concentration was 0.4 wt %. The different mass-transfer enhancement values between the nanoparticles and the large silica particles might be due to the resulting surface areas. For example, the BET surface area of the large silica particles (7 μm) was 165 m^2/g, which is much smaller than the BET surface area for the MCM41 nanoparticles. In general, the larger the silica particle surface area per unit mass, the more CO that can be physically adsorbed. Alternatively, the higher geometric surface area of nanoparticles relative to their volume might be responsible for the differences shown in Figure 3.

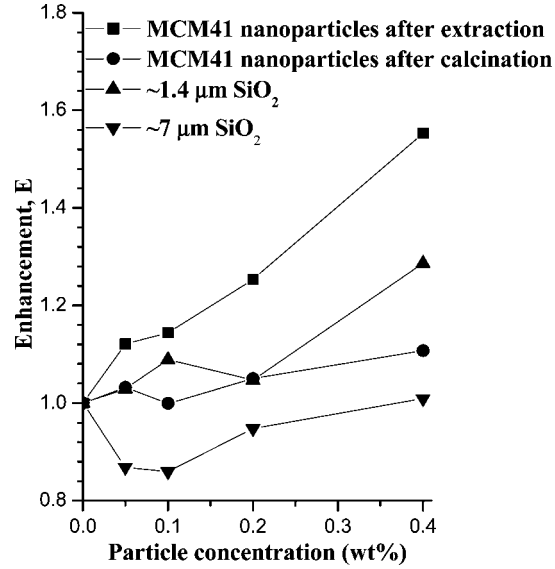

Figure 3. Enhancement of the CO−water volumetric mass-transfer coefficient for different silica samples as a function of particle concentration.

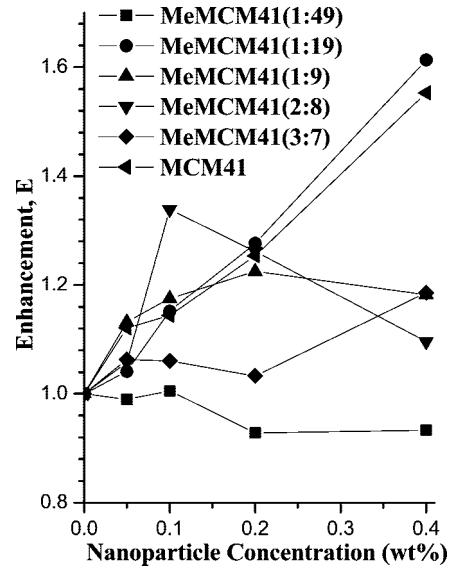

Figure 4. Enhancement of the CO−water volumetric mass-transfer coefficient with various methyl group loadings grafted to MCM41 nanoparticles as a function of nanoparticle concentration.

As shown in Figure 3, the particle preparation procedure can also influence the resulting mass-transfer enhancement. The surfactant utilized in the MCM41 preparation can be removed by extraction or calcination.[27,28] After calcination at 500 °C for 5 h with a ramp of 1 °C/min, the MCM41 nanoparticles retained their mesoporous structure, but as measured, their BET surface area decreased by ~10%. However, the maximum enhancement dropped dramatically from 1.55 for MCM41 nanoparticles after extraction to 1.11 for MCM41 nanoparticles after calcination. Extracting the surfactant from the MCM41 nanoparticles retained more surface hydroxyl groups because the process was carried out at a lower temperature (<100 °C). In contrast, calcination at a high temperature (500 °C) diminished the number of hydroxyl groups on the MCM41 surface.[29] Accordingly, the significant decrease in enhancement with the addition of MCM41 nanoparticles after calcination was primarily attributed to the removal of surface hydroxyl groups. Hence, surface hydroxyl groups play an important role in determining

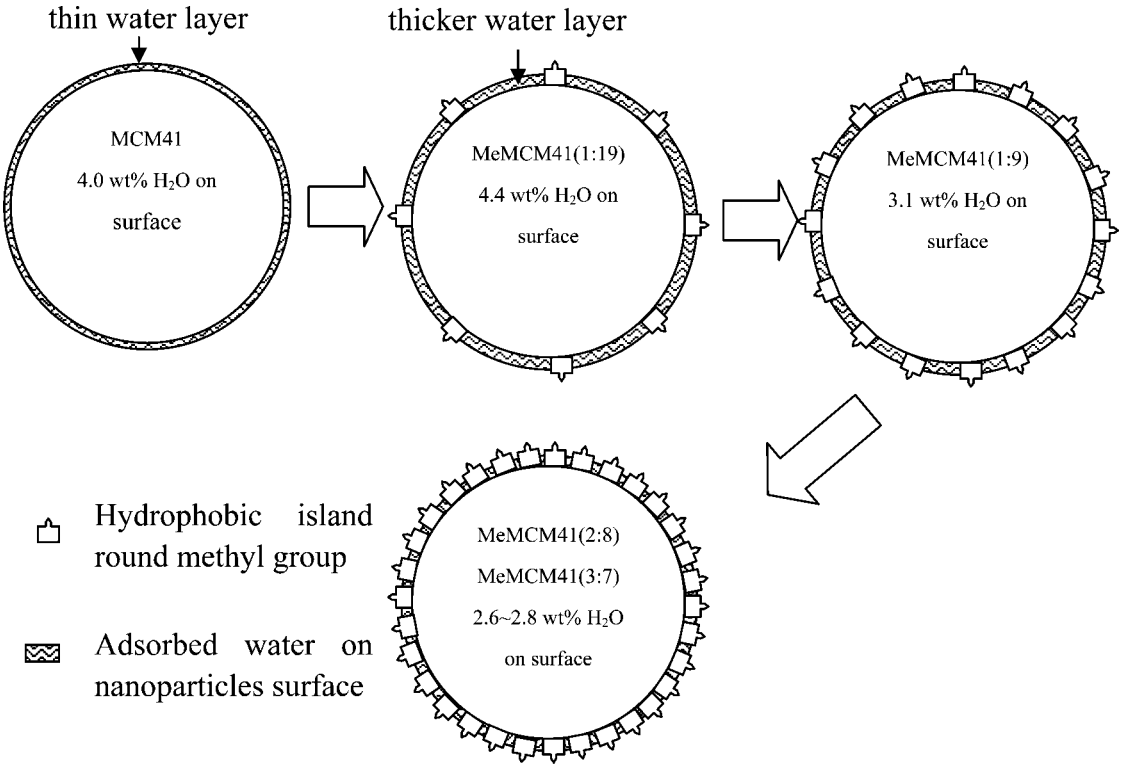

Figure 5. Proposed scheme for water adsorption on the MeMCM41 samples.

CO−water mass-transfer enhancement upon the addition of nanoparticles.

As indicated by Beenackers and van Swaaij,[20] the enhancement of small particles in gas−liquid mass transfer could be influenced by the hydrophobicity of the small particles. In this work, various methyl group loadings were grafted onto the MCM41 nanoparticles to adjust the surface hydrophobicity to study its effect on CO−liquid mass-transfer enhancement. Figure 4 shows the enhancement of the CO−water volumetric mass-transfer coefficient with various methyl group loadings as a function of nanoparticle concentration. MeMCM41(1:19) nanoparticles showed a continuous increase in enhancement with increasing nanoparticle concentration, with the highest value of $E = 1.61$ when the nanoparticle concentration was 0.4 wt %. For samples with other methyl group loadings or at other nanoparticle concentrations, the mass-transfer enhancement was on the order of 10−20%, which was generally lower than that of pure MCM41 nanoparticles. The notable exception was the MeMCM41(1:49) material, which actually decreased the mass transfer (i.e., $E < 1$).

The results above indicate that CO−liquid mass-transfer enhancement due to MCM41 nanoparticle addition is influenced by the hydroxyl groups on the nanoparticle surface. Because CO molecules can interact with, and be adsorbed by, hydroxyl groups, the extent of CO−liquid mass-transfer enhancement should depend on the number of hydroxyl groups exposed to a CO gas bubble. The number of hydroxyl groups on the nanoparticle surface is related to the methyl group loading and can be estimated by measuring the amount of water desorption from the nanoparticles by thermogravimetric analysis (TGA).[28] When different methyl group loadings were grafted onto MCM41 nanoparticles, as presented in Table 1, the physically adsorbed water on MeMCM41 increased from 4.0 to 4.4 wt % as the MeTEOS/TEOS molar ratio increased from 0 to 1:19; it then decreased from 4.4 to 2.8 wt % as the MeTEOS/TEOS molar ratio increased from 1:19 to 3:7 because of the hydrophobicity imparted by the methyl groups. When compared to pure MCM41 nanoparticles, more water was physically adsorbed on the MeMCM41(1:19) nanoparticles (4.0 wt % compared to 4.4 wt %). Because the methyl groups created locally hydrophobic regions on the MeMCM41(1:19) surface, the surface area for physically adsorbed water was much lower than that for pure MCM41 nanoparticles. Given the increase in physically adsorbed water, it is proposed that the adsorbed water on the MeMCM41(1:19) surface formed in multiple layers, as schematically shown in Figure 5, that were thicker than that with the MCM41 surface. Potentially, the physically adsorbed water multilayers saturate the surface hydroxyl groups and thereby inhibit the interaction between the surface hydroxyl groups and the CO molecules. Assuming that Figure 5 represents the physical situation, only hydroxyl groups in the hydrophobic neighborhood around the methyl groups would be exposed to the CO bubble and would be active in adsorbing CO from the bubble. For MeMCM41(1:49), the water desorption was 14.3 wt %, which was much higher than that of the other samples and was possibly caused by water entering the pore region. In general, the grafted methyl groups would be located around the pore mouth because of the interaction between the methyl groups and the surfactant; this results in the blockage of water from entering the pore. For the sample with the very low methyl group loading, water could enter the pore and be adsorbed on the inner surface, which led to the increase in water adsorption for MeMCM41(1:49). Hence, the amount of active hydroxyl groups on the surface was less than that on pure MCM41 nanoparticles, which led to the dramatic decrease in CO mass-transfer enhancement from 1.55 to 0.93. When the methyl group loading increased to 1:19, the enhancement in CO mass-transfer rate was 1.61 because of the increase in the number of active hydroxyl groups around the hydrophobic methyl groups. However, when the methyl group loading was increased further to 1:9, 2:8, and 3:7 [i.e., MeMCM41(1:9), MeMCM41(2:8), and MeMCM41(3:7), respectively], the nanoparticle surface was

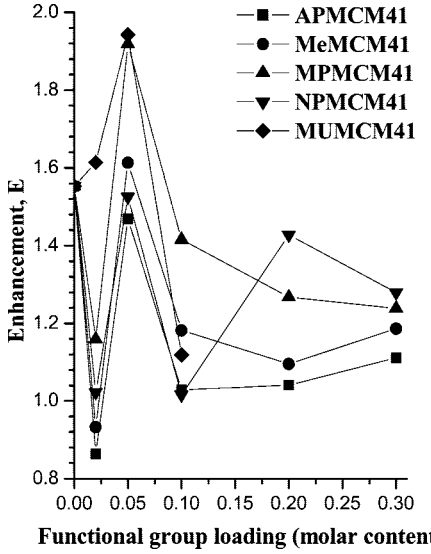

Figure 6. Enhancement of the CO−water volumetric mass-transfer coefficient when organic groups were grafted to the MCM41 nanoparticles; for all cases, the nanoparticle concentration was 0.4 wt %.

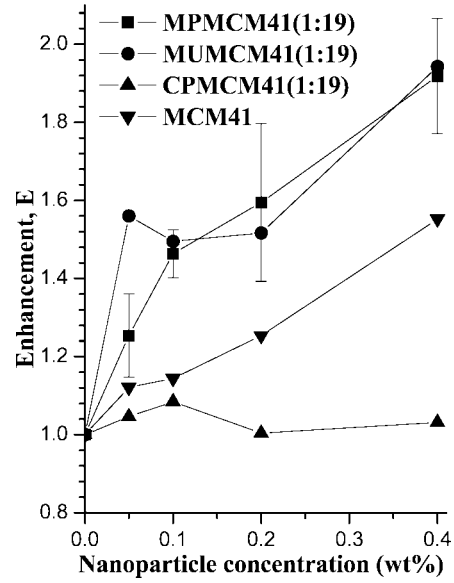

Figure 7. Enhancement of the CO−water volumetric mass-transfer coefficient for MPMCM41(1:19), MUMCM41(1:19), CPMCM41(1:19), and MCM41 as a function of nanoparticle concentration.

excessively hydrophobic and most of the nanoparticles merely floated on the water surface; this inhibited the shuttle effect of the nanoparticles and led to the decrease in the CO mass-transfer rate enhancement.

When other organic groups were grafted onto the MCM41 nanoparticles, the extent of CO−water mass-transfer enhancement was found to be a function of nanoparticle concentration, and for the conditions of this study, the strongest enhancement always occurred at the highest nanoparticle concentration (0.4 wt %). Figure 6 shows these results at a particle concentration of 0.4 wt %. When amine propyl (AP), nitrilpropyl (NP), and mercaptopropyl (MP) groups were grafted onto the MCM41 nanoparticles, the results were similar to those obtained with methyl groups grafted onto the nanoparticles; i.e., the enhancement first decreased, then reached a maximum when the propyl group molar loading was ∼5%, and then decreased with subsequent increases in propyl group loading. These results were similar to the methyl group results because the propyl groups exhibit similar hydrophobic characteristics. The notable exception to these trends was the mercaptoundecyl (MU) group, where MUMCM41(1:49) gave a much stronger enhancement than the other groups at this loading. The propyl group has three carbon atoms, whereas the undecyl group in mercaptoundecyl has 11 carbon atoms. Additionally, the undecyl group has a much larger volume than the propyl group; this increased the number of active hydroxyl groups around the undecyl group, producing an enhancement for this loading.

Figure 7 shows the enhancement of CPMCM41, MPMCM41, and MUMCM41 when the grafted organic group had a molar loading of 5%. The error bars for the MPMCM41(1:19) data represent one standard deviation from three replicate measurements. The CPMCM41 nanoparticles gave a much lower enhancement (∼1.05) compared to pure MCM41 nanoparticles. The grafted carboxylpropyl group contains a terminal carboxyl group, which has a strong hydrophilic tendency. These carboxyl groups on the MCM41 surface adsorbed more water; this led to the nanoparticle surface being completely covered with water, thereby inhibiting the interaction between the surface hydroxyl groups and CO. Hence, the CPMCM41 nanoparticles could not effectively adsorb CO from the gas bubbles and showed a negligible increase in the CO mass-transfer rate.

The maximum enhancements with MPCM41 and MUMCM41 nanoparticles were 1.91 and 1.94, respectively, which were higher than that of pure MCM41 nanoparticles. Both of these groups contain terminal mercaptan groups. Therefore, the increased enhancement appears to be related to the presence of mercaptan groups on the nanoparticle surface. Chakarov and Ho[30] investigated the interaction between CO and H_2S on a metal surface under ultrahigh-vacuum conditions. They suggested that CO can react with surface mercaptan groups generated from the decomposition of H_2S and form adsorbed OCS species. Similarly, the mercaptan groups on the MPMCM41 and MUMCM41 nanoparticle surface seemed to contribute to the adsorption of CO, which increased the CO mass-transfer rate.

It is difficult to verify the interaction between CO and the nanoparticle surface in water under the current experimental conditions because the adsorbed CO species is very unstable in water. However, the interaction between CO and the nanoparticle surface under dry conditions can be characterized by FTIR analysis using a thin, self-supporting wafer of the desired material. These results were very helpful in understanding the nanoparticle role in enhancing the CO−water mass-transfer rate. CO adsorption FTIR spectra were taken for three typical wafer samples. Figure 8 shows FTIR results for CO adsorption on MCM41, NPMCM41(2:8), and MPMCM41(2:8) wafers. The samples were all pretreated at 100 °C for 1 h in a N_2 stream to remove physically adsorbed water. Each sample was then cooled to room temperature, and CO was introduced to the system. As indicated in Figure 8, the FTIR spectra of the surface in N_2 at room temperature is identified by "r.t.". Starting at 25 °C, the spectra were taken after CO addition. After CO adsorption, a new band at ∼2041 cm^{-1} appeared in all three samples. Chin et al.[31] suggested that this band is from CO bonded linearly to the surface. Toledo-Antonia et al.[32] attributed this band to $C_{n+1}O^{2-}{}_{n+2}$ oligomeric species on the surface. Sirita et al.[33] suggested that this band corresponds to the adsorption of surface carbonyls. Despite the various opinions as to the origins of this band, it can still be concluded that the band at ∼2041 cm^{-1} originates from adsorbed CO species on the surface. When the samples were heated from 25 to 100 °C, the band diminished

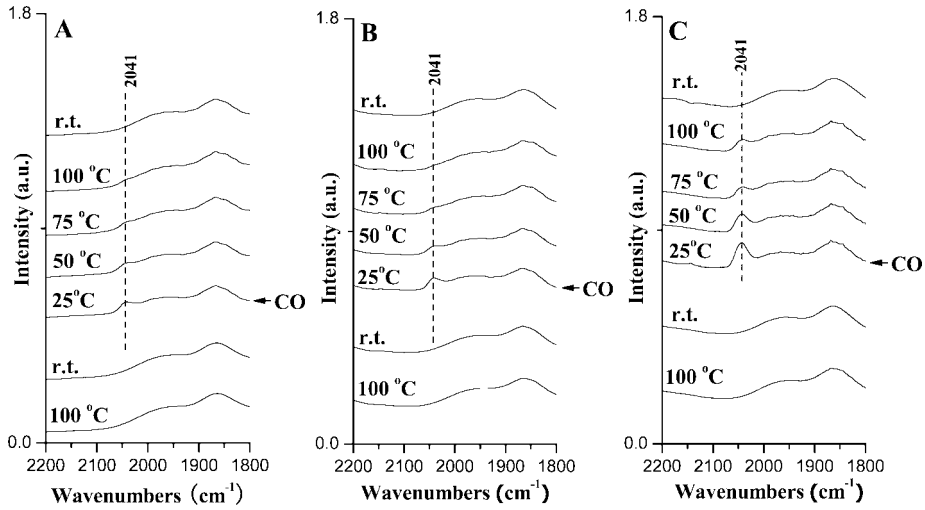

Figure 8. FTIR spectra of CO adsorbed on (A) MCM41, (B) NPMCM41(2:8), and (C) MPMCM41(2:8) wafer.

in intensity until it disappeared, which indicates that the adsorbed CO species was not very stable and decomposed with minor heating.

The adsorbed CO species was influenced by the organic group grafted to the MCM41 surface. For the MCM41 wafer, the band attributed to an adsorbed CO species disappeared at ~75 °C. However, after nitrilpropyl or mercaptopropyl groups were grafted to the MCM41 surface, the stabilization of this adsorbed CO species differed. The band attributed to an adsorbed CO species on the MPMCM41 wafer could still be detected at 100 °C (Figure 8c), which suggests that the adsorbed CO species on the MPMCM41 surface was more stable than that on the MCM41 surface. In contrast, the adsorbed CO species on the NPMCM41 wafer disappeared at ~50 °C (Figure 8b), and the band intensity was weaker than those of the MCM41 and MPMCM41 surfaces. This suggests that, for the three nanoparticle types simulated for the FTIR studies, the adsorbed CO species was most stable on MPMCM41 and least stable on NPMCM41. The band for the adsorbed CO species for MPMCM41 was also much stronger than that for MCM41 or NPMCM41, suggesting that MPMCM41 can also adsorb more CO than MCM41 or NPMCM41 under the current experimental conditions.

This result is helpful in explaining the strongest CO−water mass-transfer enhancement when mercaptopropyl or mercaptoundecyl groups are grafted onto MCM41 nanoparticles compared to other organic groups grafted onto MCM41. Hence, it is hypothesized that, when mercaptopropyl or mercaptoundecyl groups are grafted onto the MCM41 nanoparticle, the nanoparticles adsorb more CO molecules when they contact the CO bubbles, and they release these CO molecules into the water. This "catch-and-release" mechanism results in the enhancement of the CO−water volumetric mass-transfer rate.

4. Conclusions

CO−water volumetric mass-transfer coefficients were enhanced by a factor of 1.55 when ~250-nm MCM41 nanoparticles with a spherical morphology were added to the system at a loading of 0.4 wt %. Surface hydroxyl groups on the MCM41 nanoparticles played an important role in the mass-transfer enhancement, which adsorbed CO from the gas bubble and formed an adsorbed CO species. The adsorbed CO species was not very stable and readily decomposed and released CO into the water. When various organic groups were grafted onto the MCM41 nanoparticles, the interaction between the surface hydroxyl groups and the CO bubble was influenced by the functional groups. When hydrophilic groups such as carboxylpropyl were used, more water covered the nanoparticle surface and inhibited the interaction between the surface hydroxyl group and the CO gas bubble. If too many hydrophobic groups, such as methyl, amine propyl, and nitrilpropyl groups, were grafted to the nanoparticle surface, it was difficult to disperse the nanoparticles in water, and diminished enhancement was observed. For the conditions of this study, the highest CO−water mass-transfer enhancement of ~1.9 times was observed when mercaptopropyl or mercaptoundecyl groups were grafted to the MCM41 nanoparticle surface.

Acknowledgment

This material is based on work supported by the Board of Regents, State of Iowa, through the Battelle Infrastructure and Platform Grants Program. The assistance of Dr. M. Hargrove, Dr. C. Glatz, Dr. S. Jones, and Ms. S. Hruby at Iowa State University is acknowledged. Special thanks go to Dr. L. Dong at Nanjing University for the FTIR results.

Literature Cited

(1) Do, Y. S.; Smeenk, J.; Broer, K. M.; Kisting, C. J.; Brown, R.; Heindel, T. J.; Bobik, T. A.; DiSpirito, A. A. Growth of *Rhodospirillum rubrum* on synthesis gas: Conversion of CO to H_2 and poly-beta-hydroxyalkanoate. *Biotechnol. Bioeng.* **2007**, *97* (2), 279–286.

(2) Henstra, A. M.; Sipma, J.; Rinzema, A.; Stams, A. J. M. Microbiology of synthesis gas fermentation for biofuel production. *Curr. Opin. Biotechnol.* **2007**, *18* (3), 200–206.

(3) Ahmed, A.; Lewis, R. S. Fermentation of biomass-generated synthesis gas: Effects of nitric oxide. *Biotechnol. Bioeng.* **2007**, *97* (5), 1080–1086.

(4) Worden, R. M.; Bredwell, M. D.; Grethlein, A. J. Engineering issues in synthesis-gas fermentations. *Fuels Chem. Biomass* **1997**, *666*, 320–335.

(5) Lynd, L. R. Overview and evaluation of fuel ethanol from cellulosic biomass: Technology, economics, the environment, and policy. *Annu. Rev. Energy Environ.* **1996**, *21*, 403–465.

(6) Hamelinck, C. N.; Faaij, A. P. C. Future prospects for production of methanol and hydrogen from biomass. *J. Power Sources* **2002**, *111* (1), 1–22.

(7) Hamelinck, C. N.; van Hooijdonk, G.; Faaij, A. P. C. Ethanol from lignocellulosic biomass: Techno-economic performance in short-, middle- and long-term. *Biomass Bioenergy* **2005**, *28* (4), 384–410.

(8) Heiskanen, H.; Virkajarvi, I.; Viikari, L. The effect of syngas composition on the growth and product formation of *Butyribacterium methylotrophicum*. *Enzyme Microb. Technol.* **2007**, *41* (3), 362–367.

(9) Vega, J. L.; Antorrena, G. M.; Clausen, E. C.; Gaddy, J. L. Study of gaseous substrate fermentations - carbon-monoxide conversion to acetate. 2. Continuous culture. *Biotechnol. Bioeng.* **1989**, *34* (6), 785–793.

(10) Bredwell, M. D.; Telgenhoff, M. D.; Barnard, S.; Worden, R. M. Effect of surfactants on carbon monoxide fermentations by *Butyribacterium methylotrophicum*. *Appl. Biochem. Biotechnol.* **1997**, *635*, 637–647.

(11) Vega, J. L.; Clausen, E. C.; Gaddy, J. L. Study of gaseous substrate fermentations - carbon-monoxide conversion to acetate. 1. Batch culture. *Biotechnol. Bioeng.* **1989**, *34* (6), 774–784.

(12) Ungerman, A. J.; Heindel, T. J. Carbon monoxide mass transfer for syngas fermentation in a stirred tank reactor with dual impeller configurations. *Biotechnol. Prog.* **2007**, *23* (3), 613–620.

(13) Dagaonkar, M. V.; Beenackers, A. A. C. M.; Pangarkar, V. G. Absorption of sulfur dioxide into aqueous reactive slurries of calcium and magnesium hydroxide in a stirred cell. *Chem. Eng. Sci.* **2001**, *56* (3), 1095–1101.

(14) Py, X.; Roizard, C.; Bergault, I.; Midoux, N. Physical and chemical mass-transfer enhancement at a gas−liquid interface due to fine catalyst particles. *Chem. Eng. Res. Des.* **1995**, *73* (A3), 253–257.

(15) Hu, B.; Pacek, A. W.; Stitt, E. H.; Nienow, A. W. Bubble sizes in agitated air−alcohol systems with and without particles: Turbulent and transitional flow. *Chem. Eng. Sci.* **2005**, *60* (22), 6371–6377.

(16) El Azher, N.; Gourich, B.; Vial, C.; Bellhaj, M. S.; Bouzidi, A.; Barkaoui, M.; Ziyad, M. Influence of alcohol addition on gas hold-up, liquid circulation velocity and mass transfer coefficient in a split-rectangular airlift bioreactor. *Biochem. Eng. J.* **2005**, *23* (2), 161–167.

(17) Littlejohns, J. V.; Daugulis, A. J. Oxygen transfer in a gas-liquid system containing solids of varying oxygen affinity. *Chem. Eng. J.* **2007**, *129* (1−3), 67–74.

(18) Dagaonkar, M. V.; Beenackers, A. A. C. M.; Pangarkar, V. G. Enhancement of gas−liquid mass transfer by small reactive particles at realistically high mass transfer coefficients: Absorption of sulfur dioxide into aqueous slurries of $Ca(OH)_2$ and $Mg(OH)_2$ particles. *Chem. Eng. J.* **2001**, *81* (1−3), 203–212.

(19) Olle, B.; Bucak, S.; Holmes, T. C.; Bromberg, L.; Hatton, T. A.; Wang, D. I. C. Enhancement of oxygen mass transfer using functionalized magnetic nanoparticles. *Ind. Eng. Chem. Res.* **2006**, *45* (12), 4355–4363.

(20) Beenackers, A. A. C. M.; Vanswaaij, W. P. M. Mass transfer in gas−liquid slurry reactors. *Chem. Eng. Sci.* **1993**, *48* (18), 3109–3139.

(21) Schumacher, C.; Gonzalez, J.; Perez-Mendoza, M.; Wright, P. A.; Seaton, N. A. Modelling and experiment towards the design of mesoporous organic−inorganic hybrid adsorbents. In *Recent Advances in the Science and Technology of Zeolites and Related Materials, Parts A−C*; van Steen, E., Callanan, L. H., Claeys, M., Eds.; Elsevier: New York, 2004; Vol. 154, pp 386−393.

(22) Schumacher, C.; Gonzalez, J.; Perez-Mendoza, M.; Wright, P. A.; Seaton, N. A. Design of hybrid organic/inorganic adsorbents based on periodic mesoporous silica. *Ind. Eng. Chem. Res.* **2006**, *45* (16), 5586–5597.

(23) Munoz, B.; Ramila, A.; Perez-Pariente, J.; Diaz, I.; Vallet-Regi, M. MCM-41 organic modification as drug delivery rate regulator. *Chem. Mater.* **2003**, *15* (2), 500–503.

(24) Deng, W. H.; Toepke, M. W.; Shanks, B. H. Surfactant-assisted synthesis of alumina with hierarchical nanopores. *Adv. Funct. Mater.* **2003**, *13* (1), 61–65.

(25) Zhu, H. Y.; Shen, M. M.; Wu, Y.; Li, X. W.; Hong, J. M.; Liu, B.; Wu, X. L.; Dong, L.; Chen, Y. Dispersion behaviors of molybdena on titania (rutile and/or anatase). *J. Phys. Chem. B* **2005**, *109* (23), 11720–11726.

(26) Jones, S. T. Gas−liquid mass transfer in an external airlift loop reactor for syngas fermentation. Ph.D. Dissertation, Iowa State University, Ames, IA, 2007.

(27) Fowler, C. E.; Lebeau, B.; Mann, S. Covalent coupling of an organic chromophore into functionalized MCM-41 mesophases by template-directed co-condensation. *Chem. Commun.* **1998**, (17), 1825–1826.

(28) Zhao, X. S.; Lu, G. Q.; Whittaker, A. K.; Millar, G. J.; Zhu, H. Y. Comprehensive study of surface chemistry of MCM-41 using Si-29 CP/MAS NMR, FTIR, pyridine-TPD, and TGA. *J. Phys. Chem. B* **1997**, *101* (33), 6525–6531.

(29) Jin, S. M.; Qiu, G. Z.; Xiao, F.; Chang, Y.; Wan, C. F.; Yang, M. Investigation of the structural characterization of mesoporous molecular sieves MCM-41 from sepiolite. *J. Am. Ceram. Soc.* **2007**, *90* (3), 957–961.

(30) Chakarov, D. V.; Ho, W. Hot H Photochemistry of H_2S and CO Coadsorbed on Cu(111) at 68 K. *J. Chem. Phys.* **1991**, *94* (5), 4075–4077.

(31) Chin, S. Y.; Williams, C. T.; Amiridis, M. D. FTIR studies of CO adsorption on Al_2O_3- and SiO_2-supported Ru catalysts. *J. Phys. Chem. B* **2006**, *110* (2), 871–882.

(32) Toledo-Antonio, J. A.; Capula, S.; Cortes-Jacome, M. A.; Angeles-Chavez, C.; Lopez-Salinas, E.; Ferrat, G.; Navarrete, J.; Escobar, J. Low-temperature FTIR study of CO adsorption on titania nanotubes. *J. Phys. Chem. C* **2007**, *111* (29), 10799–10805.

(33) Sirita, J.; Phanichphant, S.; Meunier, F. C. Quantitative analysis of adsorbate concentrations by diffuse reflectance FT-IR. *Anal. Chem.* **2007**, *79* (10), 3912–3918.

Received for review February 08, 2008
Revised manuscript received August 5, 2008
Accepted August 12, 2008

IE800238W